Journal of Applied Physics

Terahertz topological photonic integrated circuits for 6G and beyond: A Perspective

Cite as: J. Appl. Phys. **132**, 140901 (2022); https://doi.org/10.1063/5.0099423
Submitted: 17 May 2022 • Accepted: 18 August 2022 • Published Online: 10 October 2022

Abhishek Kumar, Manoj Gupta, Prakash Pitchappa, et al.

Journal of Applied Physics PERSPECTIVE scitation.org/journal/jap

Terahertz topological photonic integrated circuits for 6G and beyond: A Perspective

Cite as: J. Appl. Phys. **132**, 140901 (2022); doi: 10.1063/5.0099423
Submitted: 17 May 2022 · Accepted: 18 August 2022 ·
Published Online: 10 October 2022

View Online Export Citation CrossMark

Abhishek Kumar,[1,2] Manoj Gupta,[1,2] Prakash Pitchappa,[3] Nan Wang,[3] Masayuki Fujita,[4] and Ranjan Singh[1,2,a)]

AFFILIATIONS

[1]Division of Physics and Applied Physics, School of Physical and Mathematical Sciences, Nanyang Technological University, Singapore 637371
[2]Centre for Disruptive Photonic Technologies, The Photonics Institute, Nanyang Technological University, Singapore 639798
[3]Institute of Microelectronics, Agency for Science, Technology and Research, 2 Fusionopolis Way, Singapore 138634
[4]Graduate School of Engineering Science, Osaka University, 1-3 Machikaneyama, Toyonaka, Osaka 560-8531, Japan

[a)]Author to whom correspondence should be addressed: ranjans@ntu.edu.sg

ABSTRACT

The development of terahertz integrated circuits is vital for realizing sixth-generation (6G) wireless communication, high-speed on-chip interconnects, high-resolution imaging, on-chip biosensors, and fingerprint chemical detection. Nonetheless, the existing terahertz on-chip devices suffer from reflection, and scattering losses at sharp bends or defects. Recently discovered topological phases of light endow the photonics devices with extraordinary properties, such as reflectionless propagation and robustness against impurities or defects, which is vital for terahertz integrated devices. Leveraging the robustness of topological edge states combined with a low-loss silicon platform is poised to offer a remarkable performance of the terahertz devices providing a breakthrough in the field of terahertz integrated circuits and high-speed interconnects. In this Perspective, we present a brief outlook of various terahertz functional devices enabled by a photonic topological insulator that will pave the path for augmentation of complementary metal oxide semiconductor compatible terahertz technologies, essential for accelerating the vision of 6G communication and beyond to enable ubiquitous connectivity and massive digital cloning of physical and biological worlds.

I. INTRODUCTION

Global digitalization, mobile Internet connectivity, and the emergence of artificial intelligence (AI) based applications have made data to be the most valuable resource. The tremendous increase in data creation and consumption demands a higher data transfer rate in both the wired and wireless domains. Nevertheless, the current rollout of fifth-generation (5G) infrastructure is just an interim solution. It cannot meet the exponentially growing demand for data consumption and massive connectivity due to bandwidth limitations. The pursuit of meeting these unprecedented demands has directed the vector toward terabits per second (Tbps) connectivity, one of the key goals for the next-generation communication network, sixth-generation (6G) communication and beyond. Terahertz (THz) frequency bands are expected to play a pivotal role in designing future high-speed wireless networks for 6G, 7G, and beyond by enabling ultrahigh bandwidth communication paradigms. The availability of huge spectral bandwidth is the key to achieving Tbps communication links without additional spectral efficiency enhancement techniques.[1,2] In addition to offering large bandwidth, THz waves encompass additional features such as (a) short wavelength, which allows for highly directional communication links and, thus, possess higher resilience to eavesdropping;[3] (b) less susceptibility to free space diffraction and inter antenna interference, which enables realization of transceiver and functional components like antennas at much smaller footprints; and (c) the pencil beam nature, which will greatly improve the angular resolution and accuracy of three-dimensional (3D) position estimation. These characteristics of THz waves provide a stepping-stone to realizing the vision of 6G and beyond to unify the physical, biological, and digital worlds by providing ubiquitous connectivity, low latency, higher energy efficiency, sensing, and high-precision 3D positioning.

However, to utilize the full potential of THz waves, it is imperative to develop integrated circuits to host hybrid electronic-photonic components on Complementary Metal Oxide Semiconductor (CMOS) compatible platform (see Fig. 1). The THz integrated circuits are essential to improve the performance and reliability of THz functional components while simultaneously reducing their size, weight, and power consumption. This will usher in high-speed on-chip communication, vital for processing and computing massive volumes of data for seamless integration of emerging communication devices with emerging 6G and beyond wireless networks. In addition, the development of THz integrated circuits will significantly alleviate the performance of a wide range of domains, such as biological diagnostics,[4,5] high-resolution imaging,[5–7] food and drugs quality inspection,[8] and nondestructive detection.[5,8] To date, the development of THz integrated circuits has been hampered due to the lack of miniaturized THz sources and detectors. Yet, the recent development of electronics[9–11] and photonics[12] based miniaturized sources open up a potential avenue for designing low-cost and highly efficient THz integrated circuits on an all-silicon (Si) platform (see Fig. 1).

To achieve high-speed data communication, *electrical*[13,14] and *optical*[13,15] interconnects are two major research areas. Among them, the electrical interconnect suffers huge Ohmic losses at THz frequencies and yields a low bandwidth-distance product. Therefore, the energy efficiency of the electrical interconnects significantly drops when transmitting the high-speed data over >1 mm due to large channel losses. Optical interconnect overcome the scaling limitations of the conventional electrical interconnect. In addition, optical interconnects offer large bandwidth. Nonetheless, the presence of various sources and electro-optical components fabricated on III–V semiconductors render the integration with the Si fabrication process and makes it cost extensive. Optical interconnects are more viable for low density and large distance communication links (tens of meters to hundreds of meters).[16]

Although, the high volume data traffic for both short distance (few centimeters and below) and long distance (tens of meters and above) communication links are well addressed by electrical[13,14] and optical[13,15] interconnects, respectively. The gap between the two regimes provides an opportunity for the insertion of a high-data rate, efficient, and cost-effective *terahertz interconnects*[16,17] into an existing ecosystem of electrical and optical interconnects to solve the "*last centimeter*"[17] problem. The performance of THz interconnects depends on the efficient integration of THz waveguiding channels with the existing photonic and electronic components. Recent works[18–22,165,166] demonstrate the integration of dielectric THz waveguide with the existing electronic and photonics-based system. In addition, recently, significant progress has also been observed in developing THz integrated circuits by combing the electronics and photonics solutions.[23,24] Arguably, the planar waveguide platform is one of the key elements for THz integrated circuits. It offers to host various passive and active components to achieve comprehensive functionalities. In this regard, different waveguide structures inspired by microwave and optics have been proposed for the THz spectral region. At THz frequencies, the conventional metallic waveguides such as microstrip lines, coplanar, hollow, and substrate-integrated waveguides suffer from huge ohmic losses that compound to transmission loss in the order of several dB/cm[25,26] or higher.[27] Thus, it is crucial to develop metal-free photonic waveguides. This has led to the development of all-dielectric THz waveguides. Inspired by guided wave optics,[28] various dielectric waveguides have been investigated that yield low transmission loss. High resistivity silicon (HR-Si) is an ideal choice of material, owing to low THz absorption and large non-dispersive refractive index.[29,30] In addition, Si ensures compatibility with standard foundry for rapid prototyping and commercial mass production. The development in the assembly process with Si devices also allows for integration with various active and passive devices for realizing THz integrated circuits, as illustrated in Fig. 1.

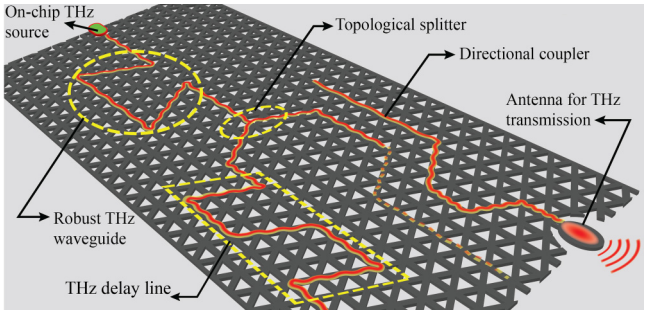

FIG. 1. Schematic of THz integrated circuits with various active (source, detector) and passive (delay line, directional coupler, antenna) components on photonic topological insulator (PTI) platform.

In the quest to develop THz integrated circuits, various dielectric waveguides have been proposed, such as unclad ribbon waveguide,[31] silicon-on-insulator (SOI) waveguides,[32–34] effective media cladded waveguide,[35] and photonic crystal waveguides.[36,37] Among them, unclad ribbon waveguides are one of the most fundamental waveguides, where the waves are confined by total internal reflection (TIR) in the orthogonal axes of wave propagation direction. These waveguides are cladded by air in both orthogonal directions and possess low loss and broad bandwidth characteristics. Despite the low loss, these uncladded ribbon waveguides have limitations in realizing THz integrated circuits due to the weak mechanical stability, lack of self-support, and support for other passive components. To improve the integrability and mechanical stability, the SOI waveguides and entirely suspended Si frame structure were proposed.[38–42] However, additional supporting material in SOI waveguides induces losses that are not negligible.[43] The losses due to the presence of substrate were minimized by excavating the portion of the substrate beneath the waveguide but at the cost of additional fabrication complexity.[32,40,44] Alternatively, to achieve mechanical stability, an anchor frame has been utilized.[38,39] Although such a frame provides mechanical strength and integrates other components, it also incurs additional scattering loss. More recently, to avoid this scattering loss, effective media cladding was used at the connection points.[38]

To avoid the losses due to the presence of mechanical fixtures and additional substrates, two-dimensional (2D) photonic crystal (PC) slab waveguides[36,37] offer a potential solution. Unlike the waveguides mentioned above, the PC slab waveguides are

self-supporting and do not require additional anchors or substrates that incur extra losses. In the 2D PC slab, the defect line acts as the waveguide where the photonic bandgap provides the in-field confinement while TIR ensures the out-of-plane confinement. One of the major limitations of PC waveguides is narrow bandwidth that restricts their adoption for wideband applications. To alleviate the PC waveguide's bandwidth limitation, a new class of self-supporting all-dielectric waveguides was recently reported using an effective medium. The effective-medium cladding was realized through the periodic perforation of the Si slab, where TIR ensures the confinement of the wave in both in-plane and out-of-plane directions.[35,45] All the above-mentioned dielectric waveguides exhibit low transmission loss and are compatible with standard planar fabrication techniques. However, they show considerable bending losses at sharp bends. This restricts their utilization for miniaturized functional components such as power splitter, on-chip directional coupler, and delay lines. Furthermore, multiple components on a single chip induce significant reflections due to the impedance mismatch, which becomes a severe problem for THz integrated circuits. One way to reduce the backscattering is to use non-reciprocal devices.[46] However, it is challenging to implement it on integrated platforms due to the weak magneto-optical effect at THz frequencies.[47,48] Thus, a paradigm shift in design is needed to develop a robust, miniaturized, low loss, and cost-effective THz integrated circuit platform.

Photonic topological insulator (PTI),[49–54] the photonic analog of electronic topological insulator (TI), opens up a new avenue for developing extremely low loss and miniaturized THz integrated circuits. The introduction of topology endows the photonic devices with unprecedented functionalities such as reflection-free transport of light and robustness against impurities or defects without backscattering.[51] With these remarkable properties, PTI is expected to bring about significant advancement to the field of THz integrated photonics. Here, we present our perspective on the field of THz PTIs. We start with a comprehensive overview of different PTIs along with basic theoretical formalism, discuss the emerging THz photonic functional devices based on PTI, and conclude with potential applications.

II. RECENT DEVELOPMENTS IN PHOTONIC TOPOLOGICAL INSULATORS

Figure 2 depicts the different types of PTI classified based on their broken symmetry. The concept of topology was first introduced in electronic systems to characterize the phase of matter.[55–58] After the discovery of the quantum Hall (QH) effect back in 1980,[59–61] quantum spin Hall (QSH),[56,57] quantum anomalous Hall (QAH),[62] and valley Hall[63–65] effects were subsequently discovered. The most remarkable feature of topological insulators (TIs) is the presence of surface edge states that are immune to disorder and impurities and hold great potential for numerous applications. The underlying physics of TIs are universal. Therefore, the analog of TI was later extended to the various domain of physics such as acoustics[66] and photonics.[49,51,53,67] In photonics, the photonic topological insulators (PTIs)[68] possess similar topological properties to their electronic counterparts, allowing light to travel through sharp bends without backreflection. This has opened a route for designing efficient photonic devices and integrated circuits.

This section briefly discusses some of the key demonstrations of topological edge states in the photonics domain. The pioneering example of the quantum Hall effect of condensed matter system was first theoretically described[69–71] and experimentally implemented in the microwave domain by utilizing the gyromagnetic ferrite rods in static magnetic fields.[53,67] The presence of a magnetic field breaks the time-reversal (TR) symmetry and enables the chiral edge mode to propagate unidirectionally at the insulating bulk boundary, as shown in Fig. 2(a). The direction of edge states depends on the magnetic field's direction, and the edge state's robustness was demonstrated by introducing a metallic impediment in the propagating path. This approach was adopted in various other experiments[72] to show the photonic analog of the quantum Hall effect. One of the significant drawbacks of quantum Hall PTI is the requirement of the external magnetic field, which puts a severe limitation on practical implementation. In addition, the magnetic property of the material degrades with frequency and cannot be adopted for THz or optical frequencies. Thus, the need to eliminate the external magnetic field has led to the development of quantum spin Hall- PTI.[73,74] The quantum spin Hall PTI preserves the TR symmetry compared to quantum Hall PTI. The photonic counterpart of quantum spin Hall requires an analog of electron spin degree of freedom and spin–orbit coupling, which is achieved by creating an artificial spin degree of freedom for photonic modes.[75,76] Various optical degree of freedom is utilized as pseudospins, such as polarization in bi-anisotropic metamaterial,[77] transverse electric (TE) and transverse-magnetic (TM) modes of photonic crystal,[74,78,79] chiralities of ring resonators,[73] and p and d orbitals of artificial photonic atoms.[76,80] On an all dielectric platform, the quantum spin Hall PTI[76] was realized by deforming the honeycomb lattice of cylinders into a triangular lattice of cylinder hexagons, shown in Fig. 2(b). Alternatively, topologically protected modes were also realized by applying periodic modulation either in space or time and are known as Floquet PTI.[81] Until now, the experimental realization of Floquet PTI has been reported in the optical regime by introducing helical structure in a 2D honeycomb lattice of coupled waveguides, as shown in Fig. 2(c).[81] The spatial modulation of waveguides is equivalent to applying fast and strong temporal modulation that generates a synthetic gauge field and leads to the opening of a photonic bandgap.[82]

The other class of PTI which exhibits a topologically protected edge is valley Hall PTI. It is a photonic analog of valleytronic material that hosts valley-dependent chiral edge states. For integrated circuits, valley Hall PTI is an ideal candidate, as it offers robust transport of light in a highly compact structure with a periodicity of the order of wavelength.[83] The broken inversion symmetry lifts the degeneracy of Dirac points in a 2D hexagonal lattice and induces non-vanishing valley-dependent Berry curvature. The Berry curvature is a quantity that characterizes the topological connection between conduction and valance band, equivalent to a magnetic field in the momentum space. The bulk-boundary correspondence ensures the valley edge states at the interface of two photonic crystals with the opposite signed Berry curvature. These edge states are robust and can bypass the sharp bends provided intervalley mixing is absent. Utilizing the properties of valley edge

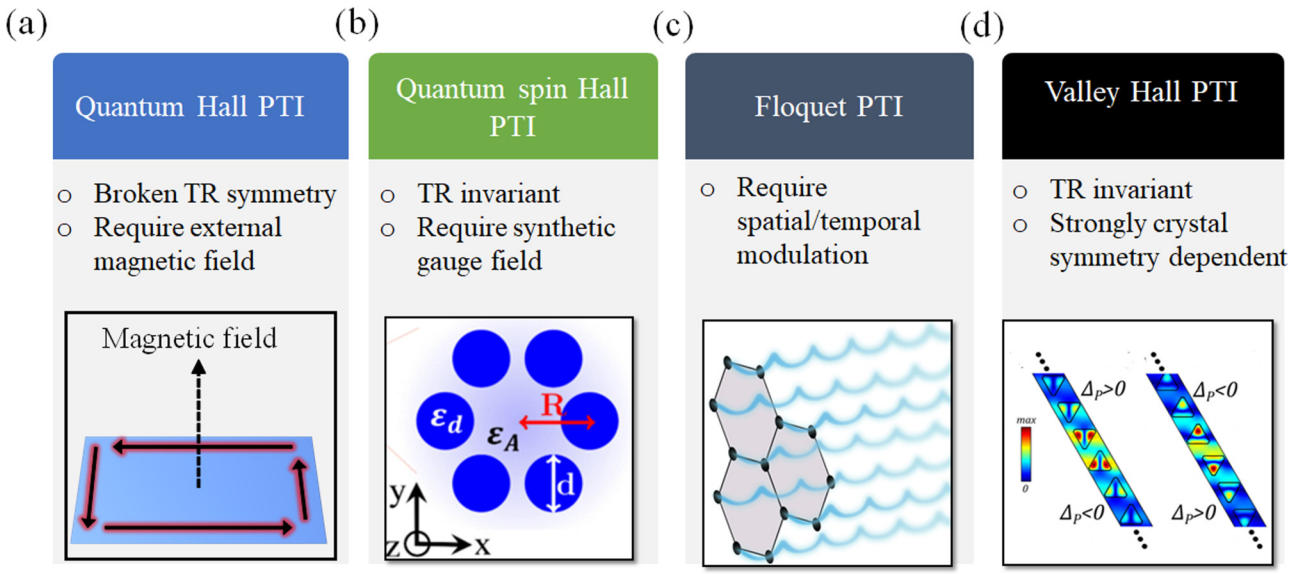

FIG. 2. Broad classification of photonic topological insulators (PTIs). (a) Quantum Hall PTI. (b) Quantum spin Hall PTI. The inset figure is reproduced with permission from Wu *et al.*, Phys. Rev. Lett. **114**, 223901 (2015). Copyright 2015 American Physical Society.[76] (c) Floquet PTI. (d) Valley Hall PTI. The inset image is reproduced with permission from Ma *et al.*, New J. Phys. **18**, 025012 (2016). Copyright 2016 Author(s), licensed under a Creative Commons Attribution (CC BY) license.

states, various optical phenomena have been demonstrated theoretically and experimentally, such as robust waveguiding,[84] Klein tunneling,[85] and valley-spin locking.[86] The concept of valley Hall PTI was recently introduced to the integrated photonics platform at telecommunication frequencies.[87–89] At THz frequencies, the topological valley photonic chip on the Si platform showed unprecedented on-chip data rates.[18,19] In addition to technological relevance, the THz topological valley photonics possess a potential outlook for exploring various fundamental phenomena such as lasing,[90–92] quantum source,[93] and topological light–matter interactions.

A. Topological invariants and edge states

Before we discuss the functional components of THz topological integrated circuits, this section briefly outlines the underlying physics of topological photonics. The idea of topology is derived from the branch of mathematics, which deals with the quantities that are preserved under continuous deformation. Mathematically, the different topologies can be characterized by an integer quantity called *topological invariants*, which remain invariant under continuous transformation and local perturbations. In the context of photonic systems, the topological invariants are defined using the dispersion bands (often called energy band diagram) in reciprocal (wavevector) space. The topological invariant of the photonic system is called Chern number[49,51] which characterizes the quantized collective behavior of the wavefunctions on the band. Photonic systems with zero Chern number are referred as the *trivial* system, while the systems with non-zero Chern number are called topologically *nontrivial*. Photonic systems with identical Chern number are topologically equivalent which means they are in the same topological phase.

The peculiar and startling phenomena occur at the interface of two topologically different systems (or an interface of a trivial and nontrivial system), where highly robust states exist. These unique states are called *edge states* that exist within the bandgap of the nontrivial photonic system. The formulation of Chern number aids to explain the occurrence of edge states. When two photonic systems with different Chern numbers are interfaced, the topology does not allow them to connect directly. A topological phase transition must occur at the interface, which requires closing the bandgap, neutralizing the Chern numbers, and then reopening the bandgap while remaining gapped in the bulks of both the photonic systems. The topological phase transition at the interface ensures the existence of gapless frequency states. If the gap remains open during the phase transition, it signifies that both the photonic systems are in same topological phase. It typically occurs for the interface between photonic systems with identical Chern numbers. In general, the opening of a bandgap is enforced by the system symmetry. Therefore, for a topological phase transition to occur, symmetry breaking must take place. In the quantum Hall photonic system, the presence of an external magnetic field breaks the time-reversal symmetry,[53] while for the valley Hall PTI,[18,83,87,88] breaking of inversion symmetry ensures valley-dependent robust edge states. Floquet PTI[81,94] induces topological effects by breaking the reciprocity through periodic time modulation.

B. Mathematical formulation of Berry curvature and Chern number

To understand the mathematical formulation, we begin with the eigenvalue problem of the periodic photonic lattice in

momentum space,

$$H(k)\psi_n(k) = \lambda_n(k)\psi_n(k), \tag{1}$$

where $\lambda_n(k)$ and $\psi_n(k)$ are the eigenvalue and normalized eigen wavefunction of Hamiltonian $H(k)$ at each k for nth band. Adiabatically changing the k-value along a given energy band results in the accumulation of non-zero phase with $\psi_n(k)$, referred as *Berry phase*.[95,96] To calculate the Berry phase, we need to add up all the phase contributions from each small change of k. The phase change of two ψ_n states separated by infinitesimal value of dk can be evaluated by their inner product as

$$\langle \psi_n(k)|\psi_n(k+dk)\rangle \approx 1 + dk\,\langle \psi_n(k)|\nabla_k|\psi_n(k)\rangle = e^{[-idk\cdot A_n(k)]}, \tag{2}$$

where we used the Taylor expansion to simplify the expression. Here, $dk \cdot A_n(k)$ accounts for the phase shift over dk and $A_n(k)$ specify the rate of change of the phase shift, popularly known as *Berry connection* or *Berry vector potential*, which can be written as

$$A_n(k) = i\,\langle \psi_n(k)|\nabla_k|\psi_n(k)\rangle. \tag{3}$$

Furthermore, to evaluate the Berry phase, we perform the closed loop integration of Berry connection over a closed path l in the k-space,

$$\phi_n = \oint_l dk A_n(k). \tag{4}$$

The Berry connection defined in Eq. (3) is not uniquely defined. With the addition of periodic phase change to the wave function $\psi_n(k)$, the Berry connection transformed. Therefore, for the ease of numerical calculation, it is crucial to define a quantity that must be invariant to any arbitrary phase change. The *Berry curvature* is that quantity, which remain invariant under any phase transformation, can be defined by taking the curl of Berry connection [Eq. (3)],

$$\Omega_n(k) = \nabla_k \times A_n(k). \tag{5}$$

Then, by using Stokes's theorem, the Berry phase can be evaluated as the integral of Berry curvature,

$$\phi_n = \int_S d^2k\,\Omega_n(k). \tag{6}$$

Now translating the above formalism of the eigenvalue problem to the 2D periodic photonic lattice [for simplicity transverse electric (TE) modes] yields the eigenvalue problem as

$$\nabla \times \left(\frac{1}{\epsilon(r)}\nabla \times H(r)\right) = \left(\frac{\omega}{c}\right)^2 H(r), \tag{7}$$

where $\epsilon(r)$ is the dielectric permittivity and $H(r)$ is the complex magnetic modes. Following the eigenvalue formalism of 2D photonic lattice, the Berry connection can be extracted as

$$A_n(k) = i\,\langle H_{n,k}|\nabla_k|H_{n,k}\rangle = i\int d^2r\, H^*_{n,k}(r)\,\epsilon(r)\nabla_k H_{n,k}(r). \tag{8}$$

Using Eq. (5), the Berry curvature for the 2D photonic lattice can be calculated as

$$\Omega_n(k_x, k_y) = \frac{\partial A^n_{k_y}}{\partial k_x} - \frac{\partial A^n_{k_x}}{\partial k_y}. \tag{9}$$

With the aid of Berry curvature, using Eq. (6), we can calculate the Berry phase that a given photonic mode (here, TE mode) can acquire for a given 2D photonic lattice. As we mentioned earlier that the topological invariant, Chern number, for the photonic systems emerges from the energy band diagram (also referred as photonic band structure). For 2D photonic lattice, the Chern number of the nth band is simply the Berry phase over the full Brillouin zone, defined as

$$C_n = \frac{1}{2\pi}\int_{BZ} d^2k\Omega_n(k_x, k_y). \tag{10}$$

To numerically calculate the Chern number of the photonic lattice, we suggest the reader to follow the review article.[68]

III. PHOTONIC TOPOLOGICAL INSULATORS FOR THz FUNCTIONAL DEVICES

The remarkable properties of PTIs create many opportunities to design various THz devices with novel properties, which is crucial for developing integrated THz solutions. Sections III A–III G present various emerging applications of PTI for THz frequencies. Figure 1 shows the artistic illustration of the THz integrated circuit that includes multiple passive (e.g., delay line, directional coupler, and antenna) and active (e.g., source and detector) components on all Si-based platforms.

A. Robust THz topological waveguide

THz is considered the next frontier for high-speed wireless communication,[97–99] and the waveguide is one of the crucial components in integrated circuits as it connects various active and passive elements. Hence, developing a low-loss platform for THz waveguiding is imperative. The unidirectional propagation and immunity toward defects of edge states make the PTI an ideal waveguiding platform for THz waves. Yang *et al.* reported the first demonstration of THz topological waveguide,[18] utilizing the valley degree of freedom of THz waves. Even with ten sharp bends, the transmission through the THz valley photonic crystal (VPC) waveguides was measured to be near unity. The THz VPC was fabricated using HR-Si (>10 kΩ cm) owing to its low loss and low dispersion at THz frequencies.[29] The VPC was realized by etching a 2D hexagonal lattice of triangular air holes in 190 μm thick HR-Si slab. The unit cell of VPC consists of an equilateral triangular hole with a side length l_1 and other inverted equilateral triangular holes with a side length l_2, as shown in Fig. 3(a). Breaking the inversion symmetry by setting $l_1 \neq l_2$ leads to opening up of bandgap at the Dirac points, i.e., at K and K' valleys.

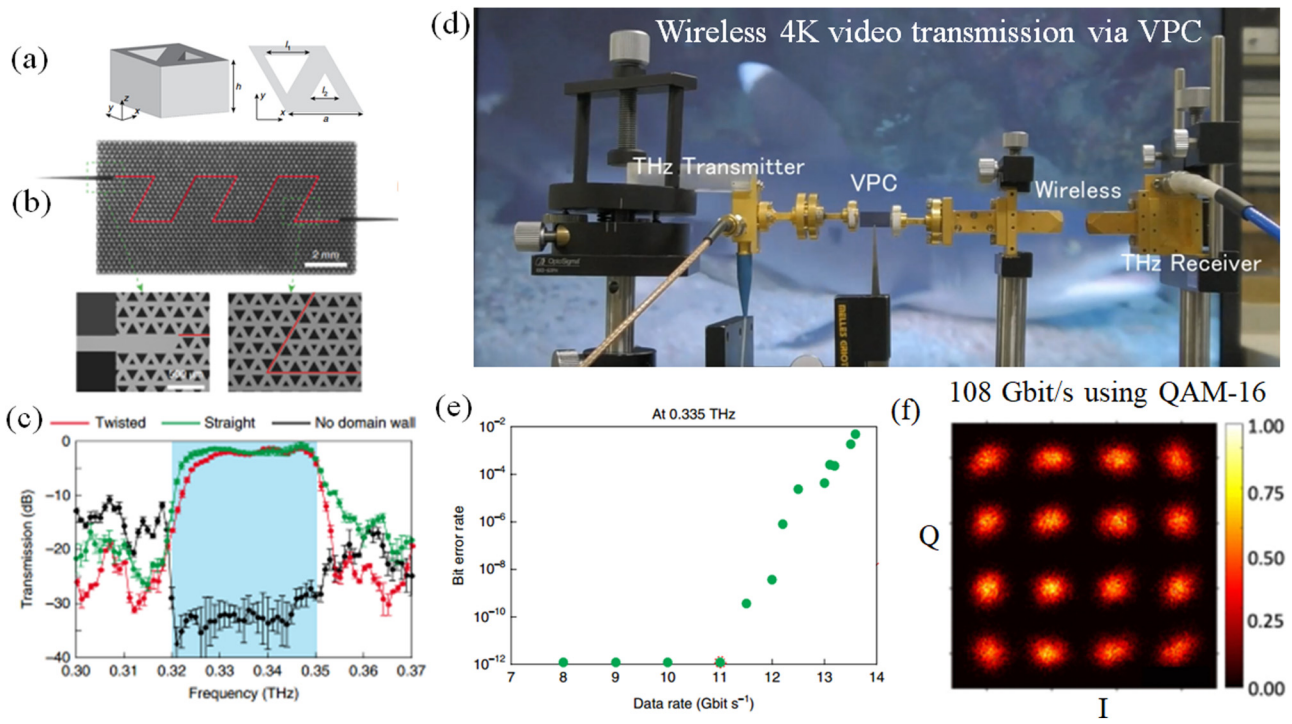

FIG. 3. Robust on-chip communication on Si-VPC (a) Unit cell of valley photonic crystal (VPC). (b) Optical image of fabricated VPC PTI waveguide. The red line shows the twisted domain wall highlighted in the inset. (c) Experimentally measured THz transmission from straight and twisted domain wall VPC. (d) Experimental setup of THz wireless communication showing transmission of uncompressed 4 K high-definition video transmission from Si-VPC chip. (e) Measured bit error rate as a function of data rate. (f) I-Q intensity constellation diagram for recovered symbols for 108 Gbit/s using QAM-16 from the Si-VPC chip. The figures in (a)–(e) are reproduced with permission from Yang *et al.*, Nat. Photonics **14**, 446–451 (2020). Copyright 2020 Springer Nature. The figure shown in (f) is reproduced and adapted with permission from Webber *et al.*, J. Lightwave Technol. **39**, 7609–7620 (2021). Copyright 2021 Author(s), licensed under a Creative Commons Attribution (CC BY) license.

Correspondingly, the Berry curvature: a "magnetic field" in momentum space becomes non-vanishing with an opposite sign at time-reversal valleys (K and K'), resulting in non-zero Chern numbers with opposite signs. This leads to zero coupling between forward propagating waves at K and backward propagating waves at K' at the domain wall: an interface formed between two VPC unit cells with opposite signed Chern number [as shown by the red line in Fig. 3(b)]. The emergence of this zero coupling is the key to achieving the robust topological waveguiding even at sharp bends. Figure 3(b) shows the fabricated VPC with ten sharp bends forming a twisted PTI waveguide. The corresponding THz transmission compared with the straight domain PTI waveguide is presented in Fig. 3(c). The negligible difference in THz transmission between the straight and twisted waveguide is the key property of PTI that allows for denser integration of THz on-chip components. Utilizing the robust nature of topological edge states, high-speed communication through a twisted VPC waveguide was also demonstrated. The THz communication setup is illustrated in Fig. 3(d). Using 0.335 THz as carrier frequency, the data rate of 11 Gbit/s with bit error rate less than 10^{-11} was experimentally demonstrated as shown in Fig. 3(e).

Furthermore, utilizing the advanced modulation scheme such as quadrature amplitude modulation (QAM), Webber *et al.*[19] has shown markedly higher data rates of 108 Gbit/s using QAM-16. Figure 3(f) shows the experimentally recorded I-Q diagram corresponding to 108 Gbit/s using QAM-16 from Si-VPC chip.

For on-chip data communication, bandwidth of the topological waveguide limits the data rate. To circumvent this, novel photonic crystal design is required that provides wide bandwidth along with topological protection. One way to achieve the wide bandwidth in VPC waveguide is by increasing the inversion symmetry. For example, by increasing the size difference of the triangular holes in VPC waveguide shown in Figs. 3(a) and 3(b), the bandwidth can be tuned.[18,19] In addition, applying the inverse design algorithms to optimize the geometrical parameters such as shape and size of the holes of VPC unit cell would be an important futuristic avenue to explore.[162]

For on-chip communication, data can be transmitted through the waveguiding channel using a carrier frequency. Reducing the presence of higher-order modes at a given carrier frequency is essential since the higher-order modes possess different propagation constants compared to the fundamental mode at a given frequency. This increases the modal dispersion, thus reducing the communication bandwidth. In addition, compared to the fundamental mode, the higher-order modes are more susceptible to radiative loss at waveguide bends due to weak confinement, thus

increasing the propagation loss. Therefore, from the communication perspective, waveguiding channel with a single allowed mode for the entire bandwidth is viable.

Another important metric that characterizes the performance of data communication through a waveguiding channel is the "dispersion" of the waveguide. Even for a single-mode transmission, a dispersive waveguiding channel leads to frequency-dependent group velocities or group refractive index that reduces the effective bandwidth of the waveguide to be used for on-chip data communication. In this regard, the edge states of the topological waveguide exhibit linear dispersion and single-mode characteristics. It reduces the mode competition and effectively allows the entire bandwidth of the topological waveguide to be used for data communication. The group delay for a signal is defined as

$$GD = -\frac{d\phi}{d\omega}, \tag{11}$$

where $d\phi$ and $d\omega$ are the change in phase (radians) and angular frequency of the signal. GD quantifies the time taken as a function of frequency for a signal to travel through the waveguiding channel. Recently, Webber *et al.*[19] has shown small group delay variation within the bandgap of the valley Hall PTI waveguide. They showed that the valley Hall PTI waveguide exhibits low group delay within the bandgap for both the straight and ten-bend waveguides. From the data communications point of view, it would be essential to develop on-demand control on tuning the GD through active modalities. To achieve this, designing an electrical gating or photo-excitation[100] could be the path forward. Note that, to access more bandwidth, carrier frequencies must increase toward upper end of the radio spectrum eventually operating up to 1 THz or beyond.[101] Also, at higher THz frequencies, the absorption loss due to free carriers in Si decreases[102] which further reduces the propagation loss on all Si-based THz components. However, to waveguide the higher frequency THz waves, thickness (T) of the Si waveguide reduces as per relation, $T = \frac{\lambda_0}{2\sqrt{n_2^2 - n_1^2}}$, where λ_0 is the wavelength of waveguiding mode and n_1 and n_2 are the refractive index of air and Si slab, respectively. As the thickness of Si slab reduces, it would be imperative to develop the THz integrated platform on SOI platform[88,103] for enhanced mechanical support and ease of integration with other functional components.

In the prospect of designing robust THz waveguides,[18,104] so far, the valley Hall PTI has been utilized. The exploration of other PTIs such as quantum spin Hall and Floquet PTIs is still lacking at THz frequencies. From the application point of view, the other PTIs may also offer important avenues. For example, the quantum spin Hall PTI can be used to sort the modes by using the "spin" degree of freedom of light. It can be further utilized to design on-chip THz spin-splitters and signal routers.

Similarly, Floquet PTI provides non-reciprocal edge states akin to quantum Hall PTI, thus offering robust transport of light. Recently, chip-scale Floquet insulator[94] based topological electromagnetic circuit with an operation frequency of 0.5 GHz has been shown for the 5G wireless system. The devised Floquet integrated circuits offer large bandwidth, strong isolation, and robustness against defects. In addition, their topological circuits are programmable and offer extreme reconfigurability, allowing them to be used in a multi-antenna full-duplex 5G wireless system. With unique features such as strong robustness, wide bandwidth, and chip-scale compatibility, Floquet PTI[105] can be utilized to develop THz topological integrated circuits for emerging 6G technologies.

B. Integrated THz topological antenna

The high free space path loss (FSPL) combined with the limited output power from the existing THz sources demand high-gain THz antennas. To efficiently utilize the THz waves for high-speed wireless communications, the THz antenna must have the following properties: (a) high directivity/gain to compensate for FSPL, (b) wide bandwidth to support large channel capacity, and (c) high efficiency to maximize radiation to free space. Application involving antenna require efficient coupling between topological waveguide modes and free space. At present, the coupling efficiency is majorly limited by a significant impedance mismatch between waveguiding modes and free space. In a recent work, Lumer and Engheta[106] have reported that utilizing topological edge states as feed lines to antenna arrays can mitigate impedance mismatch, as shown in Fig. 4(a). The absence of reflected waves in topologically protected edge states is the key to avoiding impedance mismatch, significantly simplifying the antenna design. In this context, it is also shown that the topologically protected edge states in the VPC PTI waveguide ensure reflection-free out coupling of waves. The direction of the outgoing beam depends on the effective refractive indices of valley Hall PTI.[83] For example, in a study by Ma and Shvets,[83] the authors have shown that the angle of emergence can be tuned by changing the interface of PTI waveguides, as shown in Fig. 4(b). In this study, the authors have used a hexagonal lattice of triangular holes to realize the valley Hall waveguide. $\Delta_p$is defined as the perturbation strength that is proportional ($\Delta_p \alpha\, \Delta\epsilon$) to the permittivity index contrast of the Si and air region of photonic crystal. Here, $\Delta\epsilon = \pm(\epsilon_{Si} - 1)$ is the change in permittivity after perturbation, here by etching triangular hole in the Si slab. The sign of Δ_p signifies the orientation of triangular hole. For example, the upward facing triangular hole has negative Δ_p, while downward facing has positive Δ_p. Note that, the band structures and the eigenfrequencies of the photonic crystal with opposite sign of Δ_p are identical. However, the topological indices of the propagating modes in these two photonic structures are not same. Therefore, building the valley Hall waveguide by interfacing opposite signed Δ_p photonic crystal exhibits non-identical properties, as shown in Fig. 4(b).

Following this finding, Zhang *et al.*[107] demonstrated a highly efficient directional topological acoustic antenna with less than 10° beamwidth and high directionality, as shown in Fig. 4(c). Various works have been reported on the prospect of designing THz integrated antennas by integrating the PC waveguides with dielectric resonator antenna (DRA)[108] and Luneburg lens.[109] The PTI waveguiding platform holds the potential to boost the performance of these integrated antennas due to the absence of backreflection and high-directional outcoupling owing to topological protection.

In addition to passive antenna design, the integration of phase shifters with PTI waveguide will open a whole new avenue for developing an active topological antenna. Recently, Zeng *et al.* has shown a compact, high-precision on-chip electronic THz phase shifter.[110]

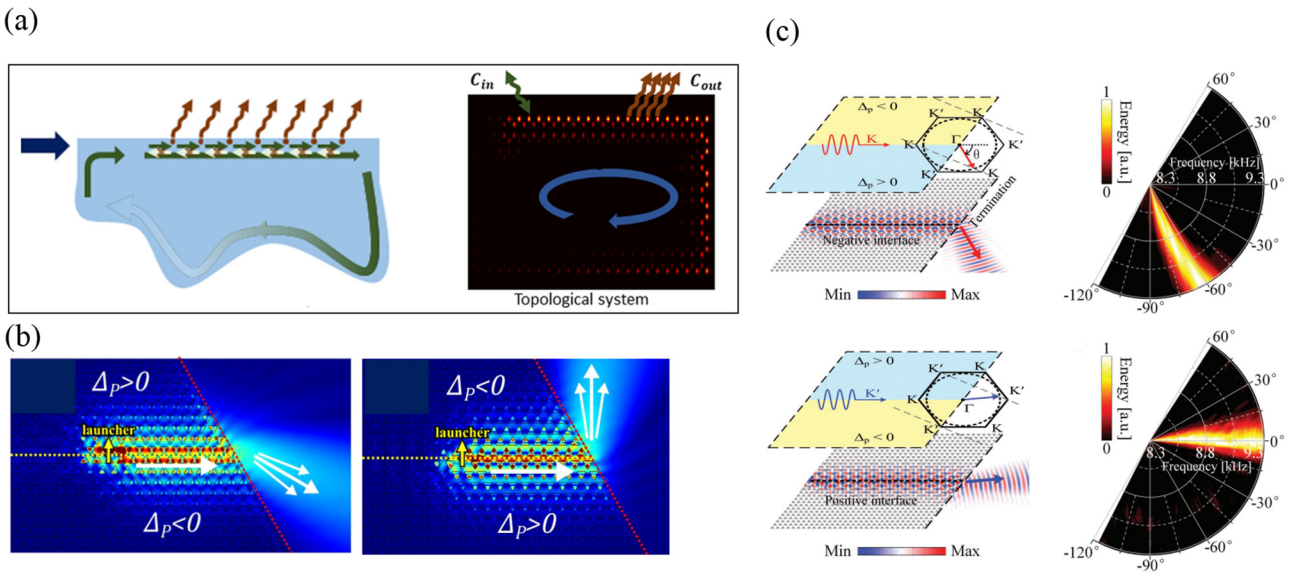

FIG. 4. Various schemes to achieve on-chip THz topological antenna. (a) Artistic illustration of topological feed line to antenna arrays. The figure is adapted from Ref. 106. Reproduced with permission from Lumer and Engheta, ACS Photonics **7** 2244–2251 (2020). Copyright 2020 American Chemical Society. (b) Outcoupling of topological edge states in valley Hall PTI. Here, Δ_p is the perturbation strength defined in Ref. 83, and by changing the interface of the PTI waveguide by combing different signed Δ_p, angle of emergence can be changed. The images are reproduced with permission from Ma *et al.*, New J. Phys. **18**, 025012 (2016). Copyright 2016 Author(s), licensed under a Creative Commons Attribution (CC BY) license. (c) Acoustic topological antenna utilized by valley Hall PTI. The angle of emergence can be tuned by changing the interface of the PTI waveguide at the end. The images are adapted from Ref. 107, Zhang *et al.*, Adv. Mater. **30**, 1803229 (2018). Copyright 2018 John Wiley and Sons.

Their devised phase shifter exhibits phase modulation without significantly affecting the amplitude of THz waves. Along this line, a similar strategy can be adopted to design an on-chip THz phase shifter on PTI waveguiding platform. By precisely controlling the phase of the THz waves in individual PTI waveguiding channels that serve as feed lines to the antenna arrays, the angle of emergence and the width of output beam can be effectively controlled.

C. Robust THz delay line

In the THz integrated circuit, the delay line is a crucial building block for various applications, including high-speed communication,[111] interferometers, imaging,[112] and time division multiplexing.[113] However, achieving broadband and long delay line with a small footprint is challenging. The traditional means to achieve delay lines are either by including long propagation length[114] or by slowing down the light using slow light effect.[115] PTI can effectively address this problem. A broadband delay line can be designed for THz frequencies by taking advantage of a topologically protected edge state. Valley Hall,[116] quantum spin Hall,[78,117] or a combination of both PTIs can be employed to engineer the THz delay line. The negligible bending loss of edge state at the sharp corner allows for tight meandering that will lead to a long delay line in a smaller footprint, as shown in Fig. 5(a). The introduction of topology for robust optical delay lines was first proposed by Hafezi *et al.*,[78] where they devised topological delay lines using a photonic quantum Hall system exhibiting robust transport of photons from the input waveguide to the output waveguide. The experimental demonstration of topological delay line in microwave frequencies was reported using quantum spin Hall PTI.[118] The schematic of delay line by introducing detour type defects in the waveguiding path is shown in Fig. 5(a). The topologically protected surface electromagnetic waves (TPSWs) are immune to backscattering at sharp corners in comparison to topologically trivial guided waves (TTGWs). Therefore, TPSW induces delay for entire bandwidth of topological waveguide, as shown in Fig. 5(b). On the other hand, TTGW reduces the operational bandwidth due to the presence of reflections [Fig. 5(b)].

Following this, a compact delay line was also proposed by integrating a topological cavity with VPC waveguide[83] as shown in Fig. 5(c). The delay time is evaluated using $\tau_{delay} = \frac{d\phi}{d\omega} - \frac{d\phi_0}{d\omega}$, where $\phi(\omega)$ and $\phi_0(\omega)$ are the frequency-dependent phase of edge states with and without the topological cavity. Figure 5(c) shows the calculated delay time for entire the bandgap region of VPC. The spectrum is normalized to $\frac{a_0}{c}$, where a_0 is the periodicity of the photonic crystal, while c is the speed of light in vacuum. Utilizing the robust transport of topological edge states, an acoustic topological delay was also devised, as shown in Fig. 5(d). Hence, PTI provides a versatile platform for realizing photonic delay lines with a small footprint. The translation of this concept to the THz frequencies holds great promise to develop on-chip THz integrated systems such as interferometers, sensors, and multiplexers.

D. THz isolator and circulator

Circulators and isolators are essential components in integrated circuits as they facilitate signal routing from transceivers and reduce the crosstalk and reflections from constituent elements.[119,120]

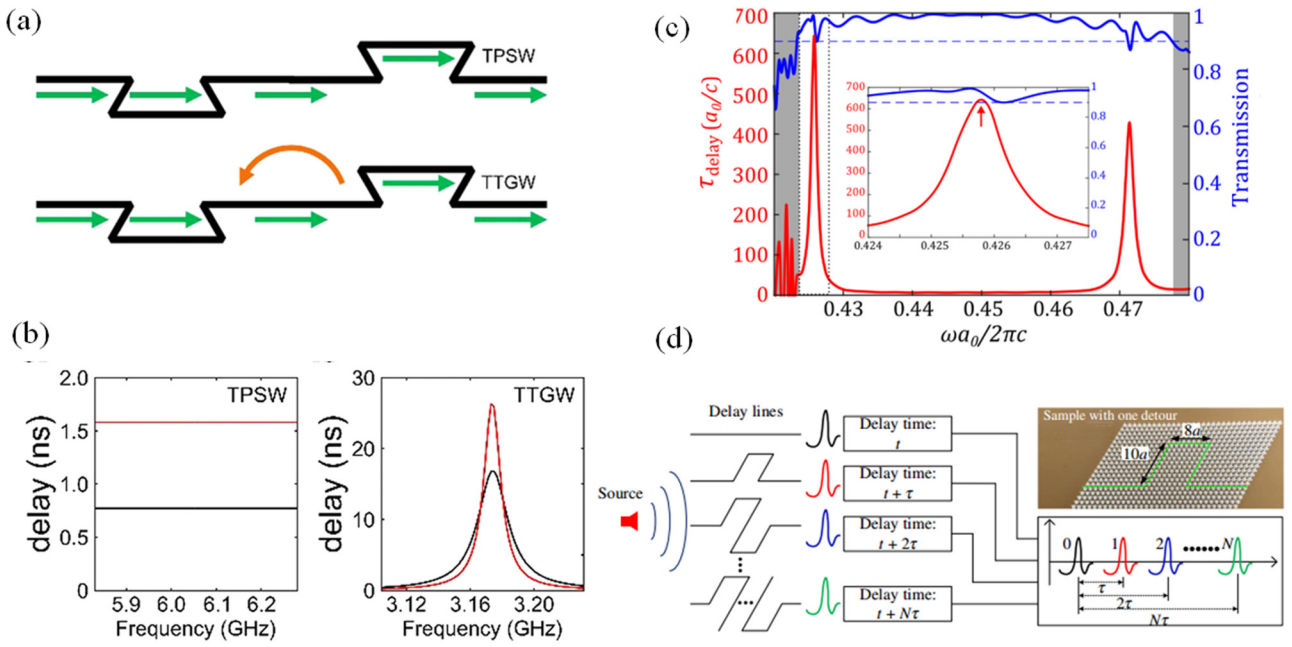

FIG. 5. Realization of delay line on various PTI platforms. (a) Schematic of robust delay line by introducing the detour defects in the waveguiding paths. (b) Two compact detours [shown in (a) produce twice the delay time (red line) compared to one detour (black line). Due to the robustness of topological edge states, the topological delay line operates for large bandwidth. On the other hand, the trivial waveguide (TTGW) exhibits reducing in operational bandwidth due to the presence of backreflections at sharp corners of detour. The images of "a" and "b" are reproduced with permission from Kueifu Lai *et al.*, Sci. Rep. **6**, 28453 (2016). Copyright 2016 Author(s), licensed under a Creative Commons Attribution (CC BY) license. (c) A realization of delay line by integrating arbitrary shaped topological cavity with valley Hall PTI waveguide. a_0 is the periodicity of the valley Hall photonic crystal and c is the speed of light in vacuum. The image is reproduced with permission from Ma *et al.*, New J. Phys. **18**, 025012 (2016). Copyright 2016 Author(s), licensed under a Creative Commons Attribution (CC BY) license. (d) An acoustic topological delay line by utilizing valley Hall PTI. Reproduced with permission from Phys. Rev. Appl. **9**, 034032 (2018).[164] Copyright 2018 American Physical Society.

Traditionally, non-reciprocal devices are used to realize these functionalities by utilizing the magneto-optical effect.[46] For example, a three-port circulator based on Si ferrite photonic crystal was numerically demonstrated in lower THz frequencies.[121] However, the weak magneto-optical effect at higher frequencies and the need for an external magnetic field limit these devices' miniaturization. In this regard, the intrinsic property of PTI robustness and unidirectionality of edge states naturally enables lossless, highly efficient, and miniaturized isolator solutions.

For circulators, recently, Ma *et* al.[122] had shown that the combination of quantum Hall and quantum spin Hall PTIs leads to three- and four-port topological circulators in the microwave region. An efficient and compact THz topological circulator could be realized by taking inspiration from microwave frequencies. In addition, the inclusion of PTI waveguides with topological cavities offers an alternate way to reroute the THz waves with topological protection.

E. Power splitter and directional coupler

Controlling the bandwidth and power along a waveguide chain is crucial in integrated circuits for various applications, including feeding networks to phased array antenna, interferometers, and signal routing. Power splitters and directional couplers serve these purposes in the integrated circuitry. Power splitters can be readily realized by bifurcating the domain wall of PTI waveguides, as shown in Fig 6(a). Compared to PC waveguides, where the power splitter requires adiabatic changes at the junction points, the negligible bending loss in PTI waveguides offers an alternative route for a smaller device footprint. In this regard, utilizing either spin or valley degree of freedom of light provides an open ground for designing robust power splitter. By judiciously designing the domain wall in topological integrated circuits, selective and robust transport of light can be achieved. As an example, Fig. 6(a) depicts a Y-junction topological power splitter where electromagnetic waves from input port 1 equally split and directed to port 2 and port 3 without backscattering even at sharp junction. Furthermore, by engineering the periodicity and structures of the topological photonic crystal by adopting an inverse design algorithm, the ratio of power splitting can be tuned arbitrarily. Recently, Cheng *et al.*[117] demonstrated a broadband splitter with topological protection as an exemplary system by utilizing the spin degree of freedom of light.

Besides, the edge states of PTI waveguides are either spin or valley selective. As an example, if the forward propagating edge states in valley Hall PTI are locked with K valley, it cannot couple with K' valley, thus by integrating the PTI waveguide with a topological cavity or mixing the PTI waveguides with different degrees of freedom, such as valley and spin [see Fig. 6(b)], THz topological

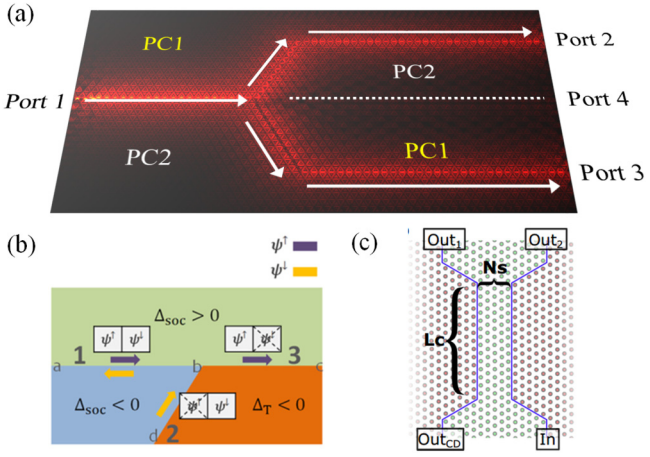

FIG. 6. Scheme to achieve power splitter and directional coupler at PTI platform. (a) Schematic of four-port topological power splitter. PC 1 and PC 2 represent the photonic crystals with opposite Chern numbers, representing different topological phases. The transport of electromagnetic waves is highlighted with red contours, localized at domain walls formed by interfacing PC 1 and PC 2. (b) Schematic of topological circulator by combing quantum spin Hall and quantum Hall PTI. Reproduced with permission from Ma *et al.*, Phys. Rev. B **100**, 085118 (2019). Copyright 2019 American Physical Society. (d) Schematic of the topological directional coupler. Reproduced with permission from Gentili *et al.*, Phys. Rev. B **100**, 125108 (2019). Copyright 2019 American Physical Society.

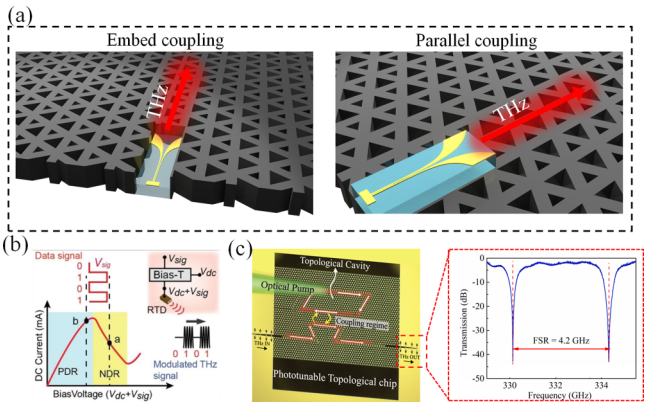

FIG. 7. THz on-chip functional components. (a) Various schemes to achieve an efficient RTD integration with THz-PTI waveguiding platform. (b) THz modulation scheme by switching RTD from NDR to PDR regions by applying an external bias voltage. (c) On-chip ultrahigh Q factor THz topological cavity and its transmission spectra. The image is reprinted with permission from Kumar *et al.*, Adv. Mater. **34**, 2202370 (2022). Copyright 2022 John Wiley and Sons.

directional coupler[122] can be realized. In microwave frequencies, Gentili *et al.*[123] demonstrated a topological directional coupler by interfacing a topological metawaveguide with a conventional circular waveguide, as shown in Fig. 6(c). So far, the experimental demonstrations are limited to microwave frequencies, its translation into the THz regime would be advantageous for on-chip functional devices.[18,124,125,153,163]

F. Integration of THz source, detector, and modulator

In the quest for developing THz integrated circuits, highly compact and efficient THz sources and detectors are essential. Along this line, various studies have been shown utilizing both electronic-photonic hybrid approach.[126,127] For example, a fully monolithically integrated transmitter which consists of lasers, optical amplifiers, modulators, and photodiodes was fabricated on Si and InP in Refs. 126 and 127. These strategies can be translated on the Si-PTI platform as well. Alternatively, resonant tunneling diode (RTD), a compact solid-state electronic device, holds the promise to deliver both the characteristic of the source and detector at room temperature.[128,129] The device footprint of RTD is smaller than 2 μm[128,129] and shown to produce THz waves with an output power of sub-milliwatts.[130] To showcase the potential of RTD, high-speed THz communication is demonstrated by integrating RTD with PC waveguides.[129,131,132] One of the key challenges in integrating RTD with the Si waveguide is efficient mode coupling and impedance matching. With the aid of a planar tapered antenna, Yu *et al.*[129] showed very high coupling (~90%) efficiency of RTD with PC waveguides. Figure 7(a) depicts various coupling schemes that could be employed to integrate RTD with PTI waveguides. With PC waveguiding platforms, several THz integrated communication modules were realized using RTD as source or detector.[36,129,131,133]

One of the added advantages of RTD is that it can also be used as THz modulators if it operates as a mixer as discussed in Ref. 132. A THz modulator is a crucial component in ultrahigh-speed communication architecture. Several recent works[134–141] have been done to enhance the modulation speed. Despite that, a miniaturized and efficient THz modulator is still lacking. By oscillating the RTD between the positive differential resistance (PDR) and negative differential resistance (NDR),[167–169] a direct THz modulation is shown. RTD acts as a THz source when it operates in NDR, as shown in Fig. 7(b) highlighted as point "a." Thus, by applying an external bias signal, RTD can be driven to operate in NDR to PDR [point "a" to "b" in Fig. 7(b)], which leads to ON/OFF modulation[144] of THz waves. Current state-of-the-art direct modulation speed of THz waves using RTD is 30 GHz.[10,145] Recently, RTD was also employed as THz receiver and demonstrated 48 Gbit/s data rate by introducing pulse amplitude modulation 4 (PAM4).[146] Hence, RTD will play a vital role in enabling miniaturized integrated transceiver solutions for enabling high-speed THz on-chip and wireless communication.[143,147]

Alternately, the photonics-based THz source uni-traveling-carrier photodiode (UTC-PD)[148,149] has also been widely adopted for high-speed THz wireless communication.[150,151] Photonics-based technology is a promising path to achieving high power and wide bandwidth THz waves. Additionally, it has the great advantage of being compatible with the existing fiber-optic network that provides a way to distribute wireless-on-fiber over a large distance.[97,152] The continuous development of semiconductor fabrication technologies will foster the monolithic integration of UTC-PD with an on-chip platform. In this regard, integrating photonics-based sources with various other active components like antenna and detectors on the Si-PTI platform will become extremely important in the future.

Interestingly, PTIs have shown remarkable advancement as a robust platform for photonic sources. In this direction, the initial works by Bandres *et al.*[92] and Harari *et al.*[91] led to the foundation for topological laser sources. Following these, Zeng *et al.* have also reported a THz quantum cascade laser by utilizing valley Hall PTI.[90] These devices are compact and robust against structural disorders like sharp bends. They used a topological cavity to enable regularly spaced robust emission peaks. In addition to lasing applications, the THz topological cavity will play an essential role in realizing spectral filters, frequency-selective signal routers, chip-scale THz spectrometers, demultiplexers, and miniaturized sensors.[153,154] Recently, a phototunable ultrahigh *Q* factor THz topological cavity [Fig. 7(c)] is realized that potentially can be used to realize on-chip THz modulator and demultiplexing devices.[163]

G. Reconfigurable THz PTI

So far, the field of topological photonics has witnessed exciting studies to design various topological phenomena and related functional devices. However, in most of these studies, the topological properties are static, and their dynamic control has remained elusive. Active control of PTI is vital for various potential applications and will enable the exploration of untapped concepts and functionalities. Recently, a few key works in the direction of reconfigurable PTI are reported using liquid crystals (LCs),[155] graphene,[156] and optical pumping.[100,157] In a theoretical proposal, the inclusion of LCs [see Fig. 8(a)] allows changing the background refractive index by changing the orientation of LCs, altering the spectral position of photonic bandgap, and topological edge states. Thus, the combination of LC with THz PTI offers a viable route to realize reconfigurable THz PTI.

Additionally, the integration of graphene with PTI offers an electrical way to tune the robust edge states. By applying electrical bias, the chemical potential of graphene can be tuned that could allow dynamic tuning of the spectral range of edge states. Furthermore, an all-optical control of the edge state was demonstrated in the valley Hall PTI[100,125,157] fabricated on all Si platform. By optically pumping, the complex permittivity of Si changed due to generation of free carriers, allowing to tune the spectral position of bandgap and topological edge states. Also, upon photoexcitation, the free carriers generated at the surface of Si allow intensity modulation of topological edge states[125,163] that potentially could be used for topological switch. Recently, with optical pumping, Kumar *et al.*[100] has shown an active tuning of coupling between a topological cavity and waveguide. By fine tuning the intrinsic losses of the topological cavity with photoexcitation, the coupling between the topological waveguide and cavity tuned from over coupled to critically coupled and under coupled regime. In the same line of dynamically controlling the topological properties of PTI, recently, an ultrafast reprogrammable plasmonic topological insulator is proposed [see Fig. 8(b)], where the topological edge states can be dynamically changed at nanoseconds time scale using PIN diodes.[158] Optical control can enable ultrafast, non-contact, and localized control, which potentially can be used for THz reconfigurable PTI. Alternate reconfigurable solutions such as integrating microelectromechanical systems (MEMS)[159] could allow an efficient THz-PTI device. Demonstrating reconfigurable THz PTI will be a significant milestone toward realizing active THz integrated circuits and will be a major research thrust in the coming decade.

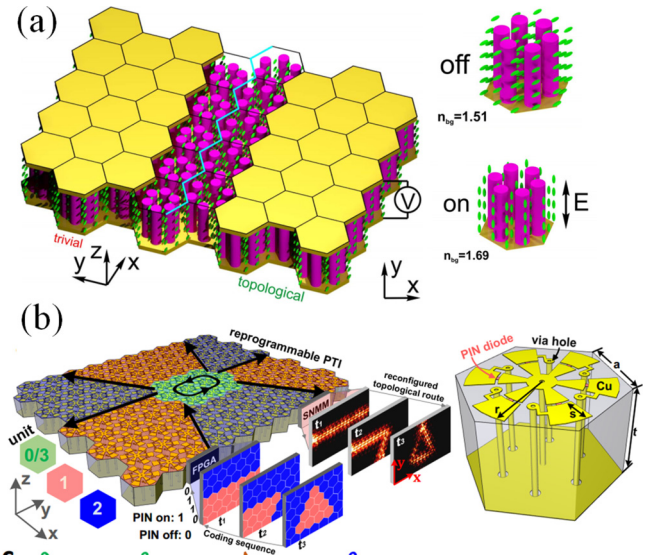

FIG. 8. Various ways to achieve reconfigurable PTI. (a) Schematic of LC integrated PTI for edge states tunability. The inset shows the different orientations of LC under the influence of an external electric field. The image is reproduced with permission from Shalaev *et al.*, New J. Phys. **20**, 023040 (2018). Copyright 2018 Author(s), licensed under Creative Commons Attribution (CC BY) license. (b) Schematic of ultrafast reprogrammable plasmonic topological insulator. Reproduced with permission from You *et al.*, Nat. Commun. **12**, 5468 (2021). Copyright 2021 Author(s), licensed under a Creative Commons Attribution (CC BY) license.

IV. CONCLUSIONS

In this Perspective, we have discussed the immense potential of the PTI platform for the technologically crucial THz spectrum. PTI holds the potential to boost the performance of existing photonic devices and offers a low loss and versatile platform for developing novel THz devices. Si has been the material of choice for realizing THz micro photonics due to the low loss, high refractive index, low dispersion, ease of fabrication, and integration with various electronic and photonic components. Such an efficient and versatile platform will be crucial for enabling a diverse range of THz functional devices, vital for next-generation high-speed wireless communication (6G communication and beyond), high-resolution imaging, and miniaturized sensors. Apart from application, PTI will be instrumental in exploring novel fundamental phenomena, such as lasing, non-Hermitian photonics, quantum photon-pair generation, quantum integrated circuits, and topological polaritonics. Also, the introduction of non-linear effects and incorporation of deep learning[160–162] into topological photonics would offer a new research direction that is expected to open the door for advanced functionalities of topological photonics, such as active tunability, bandwidth enhancement, frequency conversion, strong non-reciprocity, and entangled photon generation.

ACKNOWLEDGMENTS

A.K., M.G., P.P., N.W., and R.S. would like to acknowledge the research funding support from National Research Foundation (NRF) Singapore (Grant No. NRF-CRP23-2019-0005). M.F. acknowledges the Core Research for Evolutional Science and Technology (CREST) program of the Japan Science and Technology Agency (Grant No. JPMJCR 21C4), KAKENHI, Japan (Grant No. 20H01064), and the commissioned research by National Institute of Information and Communications Technology (NICT), Japan (Grant No. 03001).

AUTHOR DECLARATIONS

Conflict of Interest

The authors have no conflicts to disclose.

Author Contributions

Abhishek Kumar: Conceptualization (equal); Writing – original draft (equal); Writing – review & editing (equal). **Manoj Gupta:** Writing – original draft (equal). **Prakash Pitchappa:** Writing – original draft (equal); Writing – review & editing (equal). **Nan Wang:** Writing – review & editing (equal). **Masayuki Fujita:** Writing – review & editing (equal). **Ranjan Singh:** Conceptualization (equal); Writing – original draft (equal); Writing – review & editing (equal).

DATA AVAILABILITY

The data that support the findings of this study are available from the corresponding author upon reasonable request.

REFERENCES

[1]J. M. Jornet and I. F. Akyildiz, IEEE Trans Wireless Commun. **10**, 3211 (2011).
[2]T. Kürner, D. Mittleman, and T. Nagatsuma, *THz Communications: Paving the Way Towards Wireless Tbps* (Springer, 2022).
[3]J. Ma, R. Shrestha, J. Adelberg, C.-Y. Yeh, Z. Hossain, E. Knightly, J. M. Jornet, and D. M. Mittleman, Nature **563**, 89 (2018).
[4]R. M. Woodward, B. E. Cole, V. P. Wallace, R. J. Pye, D. D. Arnone, E. H. Linfield, and M. Pepper, Phys. Med. Biol. **47**, 3853 (2002).
[5]M. Tonouchi, Nat. Photonics **1**, 97 (2007).
[6]Q. Wu, T. D. Hewitt, and X. C. Zhang, Appl. Phys. Lett. **69**, 1026 (1996).
[7]S. M. Kim, F. Hatami, J. S. Harris, A. W. Kurian, J. Ford, D. King, G. Scalari, M. Giovannini, N. Hoyler, J. Faist, and G. Harris, Appl. Phys. Lett. **88**, 153903 (2006).
[8]K. Kawase, Y. Ogawa, Y. Watanabe, and H. Inoue, Opt. Express **11**, 2549 (2003).
[9]S. Iwamatsu, N. Nishigami, Y. Nishida, M. Fujita, and T. Nagatsuma, Electron. Lett. **57**, 1001 (2021).
[10]Y. Nishida, N. Nishigami, S. Diebold, J. Kim, M. Fujita, and T. Nagatsuma, Sci. Rep. **9**, 18125 (2019).
[11]T. Maekawa, H. Kanaya, S. Suzuki, and M. Asada, Appl. Phys. Express **9**, 024101 (2016).
[12]S. Jia, M.-C. Lo, L. Zhang, O. Ozolins, A. Udalcovs, D. Kong, X. Pang, R. Guzman, X. Yu, S. Xiao, S. Popov, J. Chen, G. Carpintero, T. Morioka, H. Hu, and L. K. Oxenløwe, Nat. Commun. **13**, 1388 (2022).
[13]C. A. Thraskias, E. N. Lallas, N. Neumann, L. Schares, B. J. Offrein, R. Henker, D. Plettemeier, F. Ellinger, J. Leuthold, and I. Tomkos, IEEE Commun. Surv. Tutor. **20**, 2758 (2018).
[14]J. W. Holloway, L. Boglione, T. M. Hancock, and R. Han, IEEE Trans. Microw. Theory Techn. **65**, 2373 (2017).
[15]A. V. Krishnamoorthy, K. W. Goossen, W. Jan, X. Zheng, R. Ho, G. Li, R. Rozier, F. Liu, D. Patil, J. Lexau, H. Schwetman, D. Feng, M. Asghari, T. Pinguet, and J. E. Cunningham, IEEE J. Sel. Top. Quantum Electron. **17**, 357 (2011).
[16]J. W. Holloway, G. C. Dogiamis, and R. Han, IEEE Microw. Mag. **21**, 35 (2020).
[17]Q. J. Gu, "THz interconnect: The last centimeter communication," in *IEEE Communications Magazine* (IEEE, 2015), Vol. 53, pp. 206–215.
[18]Y. Yang, Y. Yamagami, X. Yu, P. Pitchappa, J. Webber, B. Zhang, M. Fujita, T. Nagatsuma, and R. Singh, "Terahertz topological photonics for on-chip communication," Nat. Photonics **14**, 446–451 (2020).
[19]J. Webber, Y. Yamagami, G. Ducournau, P. Szriftgiser, K. Iyoda, M. Fujita, T. Nagatsuma, and R. Singh, J. Lightwave Technol. **39**, 7609 (2021).
[20]M. Ali, J. Tebart, A. Rivera-Lavado, D. Lioubtchenko, L. E. Garcia-Muñoz, A. Stöhr, and G. Carpintero, "Terahertz band data communications using dielectric rod waveguide," in *Optical Fiber Communication Conference (OFC)*, Technical Digest Series, edited by S. Matsuo, D. Plant, J. S. Wey, C. Fludger, R. Ryf, and D. Simeonidou (Optica, 2022).
[21]A. A. Generalov, D. V. Lioubtchenko, and A. V. Räisänen, "Dielectric rod waveguide antenna at 75-1100 GHz," in *2013 7th European Conference on Antennas and Propagation (EuCAP)* (EuCAP, 2013), pp. 541–544.
[22]W. Withayachumnankul, M. Fujita, and T. Nagatsuma, Adv. Opt. Mater. **6**, 1800401 (2018).
[23]K. Sengupta, T. Nagatsuma, and D. M. Mittleman, "Terahertz integrated electronic and hybrid electronic-photonic systems," Nat. Electron. **1**, 622–635 (2018).
[24]R. A. S. D. Koala, M. Fujita, and T. Nagatsuma, Nanophotonics **11**, 1741 (2022).
[25]M. Y. Frankel, S. Gupta, J. A. Valdmanis, and G. A. Mourou, IEEE Trans. Microw. Theory Techn. **39**, 910 (1991).
[26]J. Zhang and T. Y. Hsiang, J. Electromagn. Waves Appl. **20**, 1411 (2006).
[27]M. Fujishima, S. Amakawa, K. Takano, K. Katayama, and T. Yoshida, IEICE Trans. Electron. **E98.C**, 1091 (2015).
[28]S. A. Miller, M. Yu, X. Ji, A. G. Griffith, J. Cardenas, A. L. Gaeta, and M. Lipson, Optica **4**, 707 (2017).
[29]J. Dai, J. Zhang, W. Zhang, and D. Grischkowsky, J. Opt. Soc. Am. B **21**, 1379 (2004).
[30]D. Grischkowsky, S. Keiding, M. van Exter, and C. Fattinger, J. Opt. Soc. Am. B **7**, 2006 (1990).
[31]A. Malekabadi, S. A. Charlebois, D. Deslandes, and F. Boone, IEEE Trans. Terahertz Sci. Technol. **4**, 447 (2014).
[32]N. Ranjkesh, S. Gigoyan, H. Amarloo, M. Basha, and S. Safavi-Naeini, IEEE Microw. Wirel. Compon. Lett. **28**, 185 (2018).
[33]H.-T. Zhu, Q. Xue, J.-N. Hui, and S. W. Pang, "Design, fabrication, and measurement of the low-loss SOI-Based dielectric microstrip line and its components," in *IEEE Transactions on Terahertz Science and Technology* (IEEE, 2016), Vol. 6, pp. 696–705.
[34]H. Amarloo, N. Ranjkesh, and S. Safavi-Naeini, IEEE Trans. Terahertz Sci. Technol. **8**, 201 (2018).
[35]W. Gao, X. Yu, M. Fujita, T. Nagatsuma, C. Fumeaux, and W. Withayachumnankul, Opt. Express **27**, 38721 (2019).
[36]K. Tsuruda, M. Fujita, and T. Nagatsuma, Opt. Express **23**, 31977 (2015).
[37]X. Yu, M. Sugeta, Y. Yamagami, M. Fujita, and T. Nagatsuma, Appl. Phys. Express **12**, 012005 (2019).
[38]D. Headland, W. Withayachumnankul, X. Yu, M. Fujita, and T. Nagatsuma, "Unclad microphotonics for terahertz waveguides and systems," J. Lightwave Technol. **38**, 6853–6862 (2020).
[39]E. Akiki, M. Verstuyft, B. Kuyken, B. Walter, M. Faucher, J.-F. Lampin, G. Ducournau, and M. Vanwolleghem, IEEE Trans. Terahertz Sci. Technol. **11**, 42 (2021).
[40]N. Ranjkesh, M. Basha, A. Taeb, and S. Safavi-Naeini, IEEE Trans. Terahertz Sci. Technol. **5**, 280 (2015).
[41]N. Ranjkesh, M. Basha, A. Taeb, A. Zandieh, S. Gigoyan, and S. Safavi-Naeini, IEEE Trans. Terahertz Sci. Technol. **5**, 268 (2015).

[42]D. Headland, W. Withayachumnankul, M. Fujita, and T. Nagatsuma, Optica **8**, 621 (2021).
[43]K. K. Lee, D. R. Lim, L. C. Kimerling, J. Shin, and F. Cerrina, Opt. Lett. **26**, 1888 (2001).
[44]H. Amarloo and S. Safavi-Naeini, IEEE Trans. Terahertz Sci. Technol. **7**, 433 (2017).
[45]W. Gao, W. S. L. Lee, X. Yu, M. Fujita, T. Nagatsuma, C. Fumeaux, and W. Withayachumnankul, IEEE Trans. Terahertz Sci. Technol. **11**, 28 (2021).
[46]L. Bi, J. Hu, P. Jiang, D. H. Kim, G. F. Dionne, L. C. Kimerling, and C. A. Ross, Nat. Photonics **5**, 758 (2011).
[47]S. Yuan, L. Chen, Z. Wang, W. Deng, Z. Hou, C. Zhang, Y. Yu, X. Wu, and X. Zhang, Nat. Commun. **12**, 5570 (2021).
[48]M. Shalaby, M. Peccianti, Y. Ozturk, and R. Morandotti, Nat. Commun. **4**, 1558 (2013).
[49]L. Lu, J. D. Joannopoulos, and M. Soljačić, Nat. Photonics **8**, 821 (2014).
[50]A. B. Khanikaev and G. Shvets, Nat. Photonics **11**, 763 (2017).
[51]T. Ozawa, H. M. Price, A. Amo, N. Goldman, M. Hafezi, L. Lu, M. C. Rechtsman, D. Schuster, J. Simon, O. Zilberberg, and I. Carusotto, Rev. Mod. Phys. **91**, 015006 (2019).
[52]W.-J. Chen, Z. H. Hang, J.-W. Dong, X. Xiao, H.-Z. Wang, and C. T. Chan, Phys. Rev. Lett. **107**, 023901 (2011).
[53]Z. Wang, Y. Chong, J. D. Joannopoulos, and M. Soljačić, Nature **461**, 772 (2009).
[54]M. Kim, Z. Jacob, and J. Rho, Light Sci. Appl. **9**, 130 (2020).
[55]M. Z. Hasan and C. L. Kane, Rev. Mod. Phys. **82**, 3045 (2010).
[56]M. König, S. Wiedmann, C. Brüne, A. Roth, H. Buhmann, L. W. Molenkamp, X.-L. Qi, and S.-C. Zhang, Science **318**, 766, (2007).
[57]B. A. Bernevig and S.-C. Zhang, Phys. Rev. Lett. **96**, 106802 (2006).
[58]C. L. Kane and E. J. Mele, Phys. Rev. Lett. **95**, 226801 (2005).
[59]K. V. Klitzing, G. Dorda, and M. Pepper, Phys. Rev. Lett. **45**, 494 (1980).
[60]D. J. Thouless, M. Kohmoto, M. P. Nightingale, and M. den Nijs, Phys. Rev. Lett. **49**, 405 (1982).
[61]Y. Zhang, Y.-W. Tan, H. L. Stormer, and P. Kim, Nature **438**, 201 (2005).
[62]R. B. Laughlin, Phys. Rev. Lett. **50**, 1395 (1983).
[63]D. Xiao, W. Yao, and Q. Niu, Phys. Rev. Lett. **99**, 236809 (2007).
[64]H. Zeng, J. Dai, W. Yao, D. Xiao, and X. Cui, Nat. Nanotechnol. **7**, 490 (2012).
[65]J. R. Schaibley, H. Yu, G. Clark, P. Rivera, J. S. Ross, K. L. Seyler, W. Yao, and X. Xu, Nat. Rev. Mater. **1**, 1 (2016).
[66]C. He, X. Ni, H. Ge, X.-C. Sun, Y.-B. Chen, M.-H. Lu, X.-P. Liu, and Y.-F. Chen, Nat. Phys. **12**, 1124 (2016).
[67]Y. Poo, R. X. Wu, Z. Lin, Y. Yang, and C. T. Chan, Phys. Rev. Lett. **106**, 093903 (2011).
[68]D. Bisharat, R. Davis, Y. Zhou, P. Bandaru, and D. Sievenpiper, IEEE Antennas Propag. Mag. **63**, 112 (2021).
[69]S. Raghu and F. D. M. Haldane, Phys. Rev. A **78**, 033834 (2008).
[70]Z. Wang, Y. D. Chong, J. D. Joannopoulos, and M. Soljačić, Phys. Rev. Lett. **100**, 013905 (2008).
[71]F. D. M. Haldane and S. Raghu, Phys. Rev. Lett. **100**, 013904 (2008).
[72]S. A. Skirlo, L. Lu, Y. Igarashi, Q. Yan, J. Joannopoulos, and M. Soljačić, Phys. Rev. Lett. **115**, 253901 (2015).
[73]M. Hafezi, S. Mittal, J. Fan, A. Migdall, and J. M. Taylor, Nat. Photonics **7**, 1001 (2013).
[74]S. Mittal, J. Fan, S. Faez, A. Migdall, J. M. Taylor, and M. Hafezi, Phys. Rev. Lett. **113**, 087403 (2014).
[75]R. O. Umucalılar and I. Carusotto, Phys. Rev. A **84**, 043804 (2011).
[76]L.-H. Wu and X. Hu, Phys. Rev. Lett. **114**, 223901 (2015).
[77]A. B. Khanikaev, S. Hossein Mousavi, W.-K. Tse, M. Kargarian, A. H. MacDonald, and G. Shvets, Nat. Mater. **12**, 233 (2013).
[78]M. Hafezi, E. A. Demler, M. D. Lukin, and J. M. Taylor, Nat. Phys. **7**, 907 (2011).
[79]H. Kagami, H. Kagami, T. Amemiya, T. Amemiya, T. Amemiya, S. Okada, N. Nishiyama, N. Nishiyama, and X. Hu, Opt. Express **28**, 33619 (2020).
[80]S. Barik, A. Karasahin, C. Flower, T. Cai, H. Miyake, W. DeGottardi, M. Hafezi, and E. Waks, Science **359**, 666 (2018).
[81]M. C. Rechtsman, J. M. Zeuner, Y. Plotnik, Y. Lumer, D. Podolsky, F. Dreisow, S. Nolte, M. Segev, and A. Szameit, Nature **496**, 196 (2013).
[82]K. Fang, Z. Yu, and S. Fan, Nat. Photonics **6**, 782 (2012).
[83]T. Ma and G. Shvets, New J. Phys. **18**, 025012 (2016).
[84]F. Gao, H. Xue, Z. Yang, K. Lai, Y. Yu, X. Lin, Y. Chong, G. Shvets, and B. Zhang, Nat. Phys. **14**, 140 (2018).
[85]X. Ni, D. Purtseladze, D. A. Smirnova, A. Slobozhanyuk, A. Alù, and A. B. Khanikaev, Sci. Adv. **4**, eaap8802 (2018).
[86]J.-W. Dong, X.-D. Chen, H. Zhu, Y. Wang, and X. Zhang, Nat. Mater. **16**, 298 (2017).
[87]M. I. Shalaev, W. Walasik, A. Tsukernik, Y. Xu, and N. M. Litchinitser, Nat. Nanotechnol. **14**, 31 (2019).
[88]X.-T. He, E.-T. Liang, J.-J. Yuan, H.-Y. Qiu, X.-D. Chen, F.-L. Zhao, and J.-W. Dong, Nat. Commun. **10**, 872 (2019).
[89]S. Iwamoto, S. Iwamoto, S. Iwamoto, Y. Ota, and Y. Arakawa, Opt. Mater. Express **11**, 319 (2021).
[90]Y. Zeng, U. Chattopadhyay, B. Zhu, B. Qiang, J. Li, Y. Jin, L. Li, A. G. Davies, E. H. Linfield, B. Zhang, Y. Chong, and Q. J. Wang, Nature **578**, 246 (2020).
[91]G. Harari, M. A. Bandres, Y. Lumer, M. C. Rechtsman, Y. D. Chong, M. Khajavikhan, D. N. Christodoulides, and M. Segev, Science **359**, 6381 (2018).
[92]M. A. Bandres, S. Wittek, G. Harari, M. Parto, J. Ren, M. Segev, D. N. Christodoulides, and M. Khajavikhan, Science **359**, 6381 (2018).
[93]S. Mittal, E. A. Goldschmidt, and M. Hafezi, Nature **561**, 502 (2018).
[94]A. Nagulu, X. Ni, A. Kord, M. Tymchenko, S. Garikapati, A. Alù, and H. Krishnaswamy, Nat. Electron. **5**, 300 (2022).
[95]D. Xiao, M.-C. Chang, and Q. Niu, Rev. Mod. Phys. **82**, 1959 (2010).
[96]M. V. Berry, Proc. R. Soc. London A **392**, 45 (1984).
[97]S. Koenig, D. Lopez-Diaz, J. Antes, F. Boes, R. Henneberger, A. Leuther, A. Tessmann, R. Schmogrow, D. Hillerkuss, R. Palmer, T. Zwick, C. Koos, W. Freude, O. Ambacher, J. Leuthold, and I. Kallfass, Nat. Photonics **7**, 977 (2013).
[98]S. Ummethala, T. Harter, K. Koehnle, Z. Li, S. Muehlbrandt, Y. Kutuvantavida, J. Kemal, P. Marin-Palomo, J. Schaefer, A. Tessmann, S. K. Garlapati, A. Bacher, L. Hahn, M. Walther, T. Zwick, S. Randel, W. Freude, and C. Koos, Nat. Photonics **13**, 519 (2019).
[99]I. F. Akyildiz, J. M. Jornet, and C. Han, Phys. Commun. **12**, 16 (2014).
[100]A. Kumar, M. Gupta, P. Pitchappa, T. C. Tan, U. Chattopadhyay, G. Ducournau, N. Wang, Y. Chong, and R. Singh, Adv. Mater. **34**, 2202370 (2022).
[101]R. Koala, R. Maru, K. Iyoda, L. Yi, M. Fujita, and T. Nagatsuma, Photonics **9**, 515 (2022).
[102]D. K. Schroder, R. N. Thomas, and J. C. Swartz, IEEE J. Solid State Circuits **13**, 180 (1978).
[103]J. Ma, X. Xi, and X. Sun, "Topological photonic integrated circuits based on valley kink states," Laser Photon. Rev. **13**, 1900087 (2019).
[104]K. M. Devi, S. Jana, and D. R. Chowdhury, Opt. Mater. Express **11**, 2445 (2021).
[105]A. Kumar, M. Gupta, and R. Singh, Nat. Electron. **5**, 261 (2022).
[106]Y. Lumer and N. Engheta, ACS Photonics **7**, 2244 (2020).
[107]Z. Zhang, Y. Tian, Y. Wang, S. Gao, Y. Cheng, X. Liu, and J. Christensen, Adv. Mater. **30**, 1803229 (2018).
[108]W. Withayachumnankul, R. Yamada, C. Fumeaux, M. Fujita, and T. Nagatsuma, Opt. Express **25**, 14706 (2017).
[109]D. Headland, W. Withayachumnankul, R. Yamada, M. Fujita, and T. Nagatsuma, APL Photonics **3**, 126105 (2018).
[110]H. Zeng, H. Liang, Y. Zhang, L. Wang, S. Liang, S. Gong, Z. Li, Z. Yang, X. Zhang, F. Lan, Z. Feng, Y. Gong, Z. Yang, and D. M. Mittleman, Nat. Photonics **15**, 751 (2021).
[111]R. W. Boyd, D. J. Gauthier, and A. L. Gaeta, Opt. Photonics News **17**, 18 (2006).
[112]G. Yurtsever, B. Považay, A. Alex, B. Zabihian, W. Drexler, and R. Baets, Biomed. Opt. Express **5**, 1050 (2014).

[113]T. Tanemura, I. M. Soganci, T. Oyama, T. Ohyama, S. Mino, K. A. Williams, N. Calabretta, H. J. S. Dorren, and Y. Nakano, J. Lightwave Technol. **29**, 396 (2011).
[114]H. Lee, T. Chen, J. Li, O. Painter, and K. J. Vahala, Nat. Commun. **3**, 867 (2012).
[115]T. Baba, Nat. Photonics **2**, 465 (2008).
[116]H. Yoshimi, H. Yoshimi, T. Yamaguchi, T. Yamaguchi, Y. Ota, Y. Arakawa, S. Iwamoto, S. Iwamoto, and S. Iwamoto, Opt. Lett. **45**, 2648 (2020).
[117]X. Cheng, C. Jouvaud, X. Ni, S. H. Mousavi, A. Z. Genack, and A. B. Khanikaev, Nat. Mater. **15**, 542 (2016).
[118]K. Lai, T. Ma, X. Bo, S. Anlage, and G. Shvets, Sci. Rep. **6**, 28453 (2016).
[119]R. J. Potton, Rep. Prog. Phys. **67**, 717 (2004).
[120]H. Takeda and S. John, Phys. Rev. A **78**, 023804 (2008).
[121]F. Fan, S.-J. Chang, C. Niu, Y. Hou, and X.-H. Wang, Opt. Commun. **285**, 3763 (2012).
[122]S. Ma, B. Xiao, Y. Yu, K. Lai, G. Shvets, and S. M. Anlage, Phys. Rev. B **100**, 085118 (2019).
[123]G. G. Gentili, G. Pelosi, F. S. Piccioli, and S. Selleri, Phys. Rev. B **100**, 125108 (2019).
[124]Q. Yang, D. Wang, S. Kruk, M. Liu, I. Kravchenko, J. Han, Y. Kivshar, and I. Shadrivov, "Topology-empowered membrane devices for terahertz photonics," Adv. Photonics **4**(4), 046002 (2022).
[125]X. Liu, J. Huang, H. Chen, Z. Qian, J. Ma, X. Sun, S. Fan, S. Fan, Y. Sun, and Y. Sun, Photonics Res. **10**, 1090 (2022).
[126]J. Hulme, M. J. Kennedy, R.-L. Chao, L. Liang, T. Komljenovic, J.-W. Shi, B. Szafraniec, D. Baney, and J. E. Bowers, Opt. Express **25**, 2422 (2017).
[127]G. Carpintero, K. Balakier, Z. Yang, R. C. Guzmán, A. Corradi, A. Jimenez, G. Kervella, M. J. Fice, M. Lamponi, M. Chitoui, F. van Dijk, C. C. Renaud, A. Wonfor, E. A. J. M. Bente, R. V. Penty, I. H. White, and A. J. Seeds, J. Lightwave Technol. **32**, 3495 (2014).
[128]D. Headland, W. Withayachumnankul, R. Yamada, M. Fujita, and T. Nagatsuma, "Terahertz multi-beam antenna using photnic crystal waveguide and Luneburg lens," APL Photonics **3**, 126105 (2018).
[129]X. Yu, J.-Y. Kim, M. Fujita, and T. Nagatsuma, Optics Express **27**, 28707 (2019).
[130]S. Suzuki, M. Shiraishi, H. Shibayama, and M. Asada, IEEE J. Sel. Top. Quantum Electron. **19**, 8500108 (2013).
[131]X. Yu, Y. Hosoda, T. Miyamoto, K. Obata, J.-Y. Kim, M. Fujita, and T. Nagatsuma, Electron. Lett. **55**, 398 (2019).
[132]X. Yu, T. Ohira, J.-Y. Kim, M. Fujita, and T. Nagatsuma, Electron. Lett. **56**, 342 (2020).
[133]X. Yu, T. Miyamoto, K. Obata, Y. Hosoda, J.-Y. Kim, M. Fujita, and T. Nagatsuma, "Direct terahertz communications with wireless and fiber links," in *2019 44th International Conference on Infrared, Millimeter, and Terahertz Waves (IRMMW-THz)* (IEEE, 2019), pp. 1–2.
[134]A. Kumar, A. Solanki, M. Manjappa, S. Ramesh, Y. K. Srivastava, P. Agarwal, T. C. Sum, and R. Singh, Sci. Adv. **6**, eaax8821 (2020).
[135]T. C. Tan, Y. K. Srivastava, R. T. Ako, W. Wang, M. Bhaskaran, S. Sriram, I. Al-Naib, E. Plum, and R. Singh, Adv. Mater. **33**, 2100836 (2021).
[136]M. Gupta and R. Singh, "Active energy-efficient terahertz metasurfaces based on enhanced in-plane electric field density," Adv. Opt. Mater. **10**, 2200327 (2022).
[137]M. Manjappa, A. Solanki, A. Kumar, T. C. Sum, and R. Singh, Adv. Mater. **31**, 1901455 (2019).
[138]A. Kumar, Y. K. Srivastava, M. Manjappa, and R. Singh, Adv. Opt. Mater. **6**, 1800030 (2018).
[139]P. Pitchappa, A. Kumar, S. Prakash, H. Jani, R. Medwal, M. Mishra, R. S. Rawat, T. Venkatesan, N. Wang, and R. Singh, Adv. Funct. Mater. **31**, 2100200 (2021).
[140]W. X. Lim, M. Manjappa, Y. K. Srivastava, L. Cong, A. Kumar, K. F. MacDonald, and R. Singh, Adv. Mater. **30**, 1705331 (2018).
[141]P. Agarwal, L. Huang, S. Ter Lim, and R. Singh, Nat. Commun. **13**, 4072 (2022).
[142]M. Asada and S. Suzuki, *2016 IEEE International Electron Devices Meeting (IEDM)* (IEEE, Piscataway, NJ, 2016), pp. 29.3.1–29.3.4.
[143]D. Cimbri, J. Wang, A. Al-Khalidi, and E. Wasige, IEEE Trans. Terahertz Sci. Technol. **12**, 226 (2022).
[144]S. Diebold, K. Nishio, Y. Nishida, J.-Y. Kim, K. Tsuruda, T. Mukai, M. Fujita, and T. Nagatsuma, Electron. Lett. **52**, 1999 (2016).
[145]Y. Ikeda, S. Kitagawa, K. Okada, S. Suzuki, and M. Asada, IEICE Electron. Express **12**, 20141161 (2015).
[146]A. Oshiro, N. Nishigami, T. Yamamoto, Y. Nishida, J. Webber, M. Fujita, and T. Nagatsuma, IEICE Electron. Express **19**, 20210494 (2022).
[147]M. Fujita, J. Webber, and T. Nagatsuma, in *THz Communications Paving the Way Towards Wireless Tbps*, edited by T. Kürner, D. M. Mittleman, and T. Nagatsuma (Springer International Publishing, Cham, 2022), pp. 461–466.
[148]T. Ishibashi, N. Shimizu, S. Kodama, H. Ito, T. Nagatsuma, and T. Furuta, *Ultrafast Electronics and Optoelectronics (1997), Paper UC3* (Optica Publishing Group, 1997), p. UC3.
[149]T. Ishibashi and H. Ito, J. Appl. Phys. **127**, 031101 (2020).
[150]T. Harter, S. Ummethala, M. Blaicher, S. Muehlbrandt, S. Wolf, M. Weber, M. M. H. Adib, J. N. Kemal, M. Merboldt, F. Boes, S. Nellen, A. Tessmann, M. Walther, B. Globisch, T. Zwick, W. Freude, S. Randel, and C. Koos, Optica **6**, 1063 (2019).
[151]T. Nagatsuma, G. Ducournau, and C. C. Renaud, Nat. Photonics **10**, 371 (2016).
[152]H. J. Song and T. Nagatsuma, IEEE Trans. Terahertz Sci. Technol. **1**, 256 (2011).
[153]A. Kumar, M. Gupta, P. Pitchappa, Y. J. Tan, N. Wang, and R. Singh, Appl. Phys. Lett. **121**, 011101 (2022).
[154]J. C. Budich and E. J. Bergholtz, Phys. Rev. Lett. **125**, 180403 (2020).
[155]M. I. Shalaev, S. Desnavi, W. Walasik, and N. M. Litchinitser, New J. Phys. **20**, 023040 (2018).
[156]Z. Song, H. Liu, N. Huang, and Z. Wang, J. Phys. D: Appl. Phys. **51**, 095108 (2018).
[157]M. I. Shalaev, W. Walasik, and N. M. Litchinitser, Optica **6**, 839 (2019).
[158]J. W. You, Q. Ma, Z. Lan, Q. Xiao, N. C. Panoiu, and T. J. Cui, Nat. Commun. **12**, 5468 (2021).
[159]P. Pitchappa, A. Kumar, H. Liang, S. Prakash, N. Wang, A. A. Bettiol, T. Venkatesan, C. Lee, and R. Singh, Adv. Opt. Mater. **8**, 2000101 (2020).
[160]Y. J. Tan, C. Zhu, T. C. Tan, A. Kumar, L. J. Wong, Y. Chong, and R. Singh, Opt. Express **30**, 27763 (2022).
[161]J. Yun, S. Kim, S. So, M. Kim, and J. Rho, Adv. Phys. X **7**, 2046156 (2022).
[162]Y. J. Tan, W. Wang, A. Kumar, and R. Singh, "Interfacial topological photonics: Broadband silicon waveguides for THz 6G communication and beyond," Opt. Express **30**, 33035–33047 (2022).
[163]Kumar, A., Gupta, M., Pitchappa, P. *et al.* Phototunable chip-scale topological photonics: 160 Gbps waveguide and demultiplexer for THz 6G communication. Nat Commun **13**, 5404 (2022).
[164]Z. Zhang, Y. Tian, Y. Cheng, Q. Wei, X. Liu, and J. Christiensen, "Topological acoustic delay line," Phys. Rev. Appl. **9**(3), 034032 (2018).
[165]H. Aghasi, S. M. H. Naghavi, M. Tavakoli Taba, M. A. Aseeri, A. Cathelin, and E. Afshari, "Terahertz electronics: Application of wave propagation and nonlinear processes," App. Phys. Rev. **7**, 021302 (2020).
[166]T. Nagatsuma, G. Ducournau, and C. Renaud, "Advances in terahertz communications accelerated by photonics," Nature Photon **10**, 371–379 (2016).
[167]M. Asada, Jpn. J. Appl. Phys. **47**, 4375 (2008).
[168]M. Fujita, J. Webber, and T. Nagatsuma, *RTD Transceiver Project*, Springer Series in Optical Sciences, edited by T. Kürner, D. M. Mittleman, and T. Nagatsuma (Springer, 2022), Vol. 234.
[169]D. Cimbri, J. Wang, A. Al-Khalidi, and E. Wasige, "Resonant tunneling diodes high-speed terahertz wireless communications - A review," in *IEEE Transactions on Terahertz Science and Technology* (IEEE, 2022), Vol. 12, pp. 226–244.